Available online at www.sciencedirect.com
SCIENCE DIRECT®
Geochimica et Cosmochimica Acta 70 (2006) 1388–1401
Geochimica
www.elsevier.com/locate/gca

Redox reactions between iron and quinones: Thermodynamic constraints

Minori Uchimiya *, Alan T. Stone

Department of Geography and Environmental Engineering, Johns Hopkins University, Baltimore, MD 21218, USA

Received 3 August 2005; accepted in revised form 22 November 2005

Abstract

Iron is the most abundant redox-active metallic element on the earth's surface. Quinones, a term that encompasses dihydroxybenzenes (catechol and hydroquinone), semiquinone radicals, and benzoquinones, are abundant moieties within natural organic matter. Separately or in concert, iron species (both dissolved and precipitated) and quinones are believed to be key participants in a wide range of environmental redox reactions. Here, we investigate how pH, quinone structure, and iron speciation impose thermodynamic constraints on possible reactions. The steps outlined in this work must be followed to evaluate whether postulated redox processes involving iron and quinones are energetically feasible.

1. Introduction

The term quinone collectively refers to organic structures in three oxidation states linked by one-electron redox reactions. Fig. 1 illustrates *para*-quinone structures; hydroquinone (*p*-dihydroxybenzene, with three protonation levels denoted as XH_2^0, XH^-, and X^{2-}) is the fully reduced form, the *p*-semiquinone radical (with two protonation levels $YH^{\cdot}$ and $Y^{\cdot -}$) is an intermediate oxidation state, and *p*-benzoquinone (with one protonation level denoted as Z^0) is the fully oxidized form. Corresponding *ortho*-quinone structures are shown below:

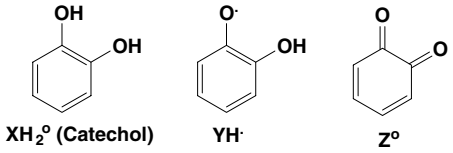

Electronic coupling of *o*- and *p*-substituents via resonance yields facile and in many instances reversible electron transfer. In contrast, meta-substituted forms do not possess this same level of resonance, do not engage in reversible two-electron transfer, and hence are not classified as quinones. The fully reduced (Dressler, 1994) and intermediate (Musso, 1967) oxidation states are shown below:

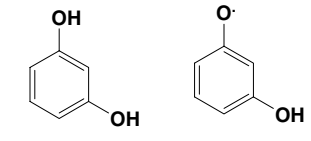

The fully oxidized form (Z^0), if present in aqueous media, would possess an extremely unstable diradical nature (Berson, 1988).

NOM is believed to contain significant amounts of quinone moieties, arising from the degradation and biological reworking of plant tissue (Thorn et al., 1992). Reversible

* Corresponding author. Present address: Division of Ecosystem Sciences, University of California, Berkeley, CA 94720, USA. Fax: +1 510 643 2940.
E-mail address: uchimiya@nature.berkeley.edu (M. Uchimiya).

0016-7037/$ - see front matter © 2005 Elsevier Inc. All rights reserved.
doi:10.1016/j.gca.2005.11.020

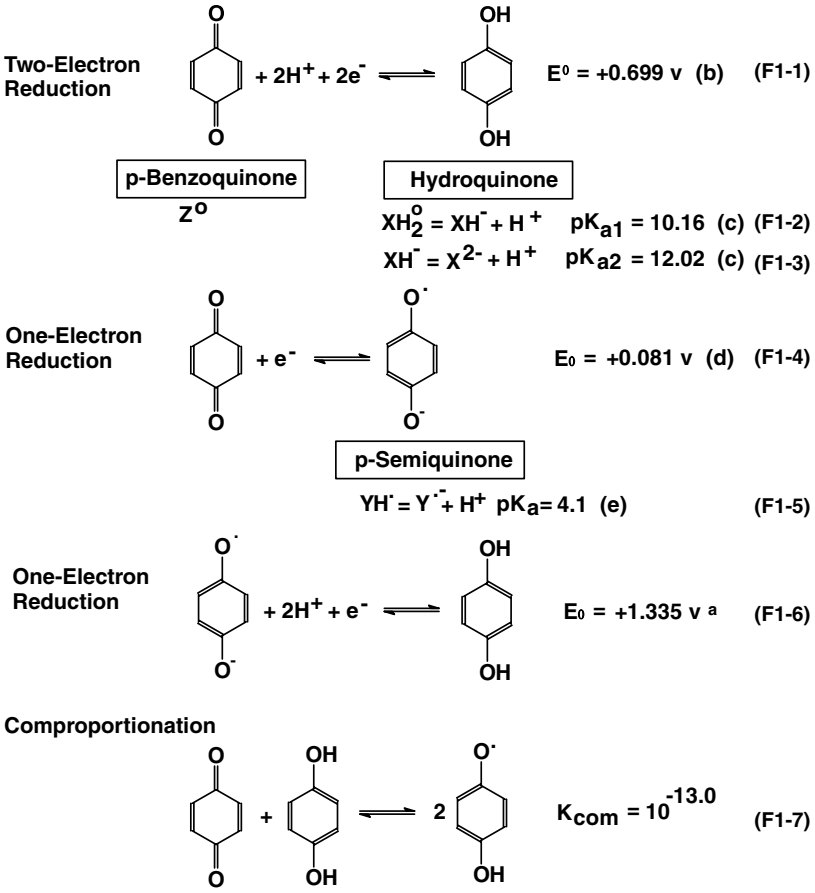

[a]Calculated using $E^0(Y^{\cdot}/X^{2-})$ (Rich and Bendall, 1980) and pK_{a1} and pK_{a2} in Table 1.

[b]Clark, 1960. [c]Martell et al., 2004. [d]Steenken and Neta., 1982. [e]Depew and Wan, 1988.

Fig. 1. *Para*-quinone structures. (See above-mentioned references for further information)

redox transformations of NOM have been attributed to the ability of quinone moieties to form stable semiquinone radicals (Scott et al., 1998; Nurmi and Tratnyek, 2002). Quinones such as juglone and lawsone are released by plants as allelochemicals (Vyvyan, 2002). It has been postulated that quinones serve as extracellular electron shuttles for microbial iron respiration (Lovley et al., 1996) and contaminant degradation (Schwarzenbach et al., 1990). Historically, anthraquinone-2,6-disulfonate (AQDS) has been employed as a model quinone moiety of NOM due to its stability towards irreversible side reactions, low standard reduction potential, high water solubility, and the convenience of analysis using UV-visible spectrophotometry. However, the actual quinone structures present in a given environment are largely unknown.

Iron is the most abundant redox-active metal ion in terrestrial ecosystems (Sposito, 1989). Microbial iron respiration is made possible by the fact that Fe^{III} (hydr)oxides, although not particularly strong oxidants, are nevertheless thermodynamically capable of oxidizing a wide range of organic substrates (Lovley, 2001). As a reductant, Fe^{II} is strong in a thermodynamic sense and reactive in a kinetic sense. Fe^{II} reduces naturally occurring compounds such as $Mn^{III,IV}$ (hydr)oxides (Postma and Appelo, 2000), and contaminants such as oxime carbamate pesticides (Strathmann and Stone, 2001) and nitroaromatic compounds (Kalusen et al., 1995).

A balanced chemical reaction is provided below for the reduction of *p*-benzoquinone (Z^0) to hydroquinone $XH_2{}^0$ by Fe^{II} under near-neutral conditions with amorphous Fe^{III} hydroxide as the solubility-limiting phase.

$$Z^0 + 2Fe^{2+} + 6H_2O = XH_2{}^0 + 2\,Fe^{III}(OH)_3(s,amorph) + 4\,H^+ \quad (1)$$

Equilibrium constants and mass balance equations are needed to account for the chemical speciation of quinones and iron dictated by protonation, coordination chemistry, and precipitation/dissolution. An equivalently useful way of addressing a redox reaction is to break a "full" reaction (Eq. (1)) into two "half" reactions for quinone (Eq. (2)) and iron (Eq. (3)):

$$Z^0 + 2H^+ + 2e^- = XH_2{}^0 \quad (2)$$

$$Fe^{III}(OH)_3(s,amorph) + 3H^+ + e^- = Fe^{2+} + 3H_2O \quad (3)$$

Reduction potentials (E in volts), calculated using the Nernst equation (Laidler and Meiser, 1999), allow the energetics of each half-reaction to be evaluated separately. The half-reaction pair with higher reduction potential is thermodynamically capable of oxidizing the half-reaction pair with the lower reduction potential. The reaction reaches equilibrium when reduction potentials of the two systems are equal to one another. For organic compounds, the comparison of reduction potentials allows us to document substituent effects and structure–reactivity relationships (Bailey et al., 1983; Bailey and Ritchie, 1985). For inorganic compounds, effects of chelation and other changes in speciation can be explored (Stone, 1997).

Plants, fungi, and bacteria release aliphatic carboxylic acids to acquire micronutrients, sequester toxic metals, and establish electrochemical gradients (Jones, 1998). Within the rhizosphere, the portion of soil in close proximity to plant roots, oxalic acid, citric acid, and other aliphatic carboxylic acids are found at concentrations as high as 1.0 mM (Sposito, 1989). The deprotonated forms of these acids possess anionic oxygen Lewis Base groups, which form complexes with Fe^{III} with higher complex formation constants than with Fe^{II}. By stabilizing Fe^{III}, oxygen-containing ligands lower the reduction potential for Fe^{III}/Fe^{II} half-reaction, making the oxidation of Fe^{II} more thermodynamically favorable. Rates of Fe^{II} oxidation by Cr^{VI} (Buerge and Hug, 1998) and oxime-carbamate pesticides such as oxamyl (Strathmann and Stone, 2002) have been found to correlate with Fe^{III}/Fe^{II}reduction potential.

Quinones, Fe^{III}/Fe^{II}, and aliphatic carboxylic acids likely coexist within many soils and sediments. Here, our objective is to consider thermodynamic aspects of redox reactions involving these chemical constituents. The redox chemistry of quinones and iron will be developed separately, then redox reactions between them will be considered. Effects of quinone functional groups, precipitation/dissolution, and complex formation by aliphatic carboxylic acids will be explored. By quantitatively accounting for each factor controlling reaction energetics, it is possible to predict the direction and extent of quinone-iron redox reactions. Subsequent papers in this series explore in detail the kinetics of these redox processes.

2. Sources of thermodynamic information and calculation procedures

All model quinone structures used in this study are listed in Table 1 with corresponding equilibrium constants. Stability constants for the iron hydrolysis reactions and solubility product constants for amorphous Fe^{II} and Fe^{III} hydroxides are provided in Table 2. Stability constants for Fe^{II} and Fe^{III} complexes with malonate and oxalate are given in Table 3.

In order to separately address the reactant speciation and the extent of reaction, calculations were performed in two distinctive steps. In the first step, half-reactions for possible redox reactants were examined. Concentrations of both oxidized and reduced form of quinone or iron system are specified, and their acid–base speciation was calculated using HYDRAQL (Papelis et al., 1988) equilibrium speciation software. To calculate the reduction potential (E) for the half-reaction being considered, outputs from HYDRAQL calculation were inserted into an appropriate Nernst equation using the Microsoft Excel software. The outcomes of the calculation procedures described above are acid–base speciation diagrams and E versus pH diagrams for quinone and iron reactants.

After examining the half-reactions of the reactants, the following "full" reactions were considered: redox reactions between different quinone structures (cross reaction), and redox reactions between quinones and iron. Again, concentrations of reactants were specified and their acid–base speciation was determined using HYDRAQL. Outputs from HYDRAQL calculations were inserted into electron balance and mass balance equations addressing the full reaction being considered. The extent of full reaction was evaluated by the product concentration, which was determined by the iteration of two or more equations using Excel. The calculation procedures described above allow us to construct a plot of product concentration versus pH for the "full" reaction under consideration.

3. Reactant description

3.1. Quinones without Lewis base side-groups

In order to provide a complete description of protonation speciation, we use different abbreviation letters for fully oxidized (Z), intermediate (Y), and fully reduced (X) oxidation states. Dihydroxybenzenes are fully protonated under acidic conditions XH_2^0, but successively lose protons, forming XH^- and X^{2-}, as the pH is increased. Comparison of first (pK_{a1}) and second (pK_{a2}) acid dissociation constants for catechol, hydroquinone (Table 1), and resorcinol ($pK_{a1} = 9.52$; $pK_{a2} = 11.50$ (Martell et al., 2004)) reveals the following trends:

pK_{a1} values: hydroquinone > resorcinol ≅ catechol
pK_{a2} values: catechol > hydroquinone > resorcinol

The two OH groups in catechol and hydroquinone are coupled to one another through resonance interactions, while the two OH groups in resorcinol are not. In addition, hydrogen bonding takes place within XH^- form of catechol, but not in hydroquinone and resorcinol. The hydrogen bonding interaction in catechol stabilizes XH^- relative to XH_2^0 and X^{2-}. As a consequence, catechol exhibits the lowest value of pK_{a1} and the highest value of pK_{a2}.

We now turn our attention to electron transfer equilibria. The fully oxidized and fully reduced forms of a quinone are linked through the half-reaction described in Eq. (2). The corresponding Nernst equation is given below:

Table 1
Names, structures, standard reduction potentials (E^0)[a], and acid dissociation constants (pK_a)[b] of model quinones

Name	Structure(oxidized form; Z^0)	Structure(reduced form; $XH_2{}^0$)	E_0 (volts)	pK_{a1}	pK_{a2}
o-Benzoquinone (Z^0) Catechol ($XH_2{}^0$)	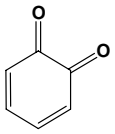	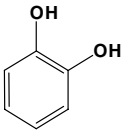	0.803[c,e]	9.45[f]	13.74[f]
Chloro-*p*-benzoquinone (Z^0) Chlorohydroquinone ($XH_2{}^0$)	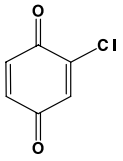	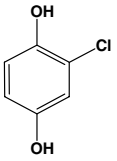	0.712[e]	9.2[g]	11.61[g]
p-Benzoquinone (Z^0) Hydroquinone ($XH_2{}^0$)	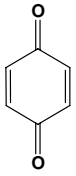	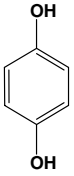	0.699[c,e]	10.16[f]	12.02[f]
Homogentisic acid ($XH_2{}^0$) Benzoquinonacetic acid (Z^0)	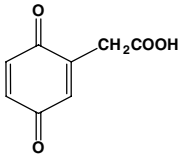	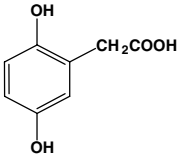	0.687[e]	N/A pK_{aR} 4.30[e]	N/A pK_{aZ} 3.30[e]
2,5-Dimethyl-*p*-benzoquinone (Z^0) 2,5-Dimethyl-hydroquinone ($XH_2{}^0$)	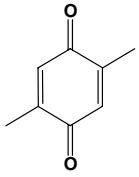	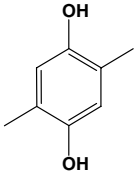	0.593[e]	10.68 [h]	13.11[g]
5-Hydroxy-naphtho-hydroquinone ($XH_2{}^0$) Juglone (Z^0)	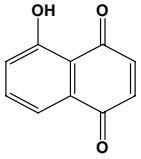	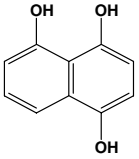	0.428[e]	10.60[i] pK_{aR} 6.60[e]	N/A pK_{aZ} 8.00[e]
Anthraquinone-2,6-disulfonate (AQDS Z^0) Anthrahydroquinone-2,6-disulfonate ($XH_2{}^0$)	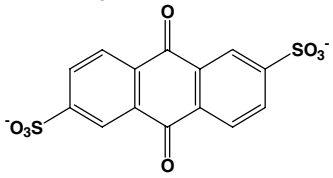	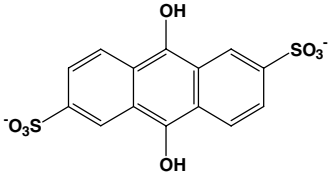	0.228[d,e]	8.1[e]	10.5[e]

[a] E_0 represents the standard reduction potential for the following reaction: $Z^0 + 2H^+ + 2e^- = XH_2{}^0$. Unless otherwise noted, no activity corrections were made.

[b] Corrected to zero ionic strength using the Davies equation (Stumm and Morgan, 1996). pK_{a1} and pK_{a2} represent first and second acid dissociation constants for -OH groups of the dihydroxybenzene. pK_{aR} and pK_{aZ} represent acid dissociation constants of substituents on the reduced and oxidized form, respectively.

[c] Corrected to zero ionic strength using the Davies equation (Stumm and Morgan, 1996).

[d] For fully protonated species of both oxidized and reduced forms.

[e] Clark (1960).

[f] Martell et al. (2004).

[g] Clemmer et al. (1979).

[h] Fukuzumi et al. (1989).

[i] Deiana et al. (1995).

Table 2
Stability constants[a] for Fe^{II} and Fe^{III} hydrolysis reactions

Equilibrium expression	Log K[b]
$Fe^{2+} + H_2O - H^+ = Fe^{II}OH^+$	−9.397
$Fe^{2+} + 2H_2O = Fe^{II}(OH)_2{}^0 + 2H^+$	−20.494
$Fe^{2+} + 3H_2O = Fe^{II}(OH)_3{}^- + 3H^+$	−28.494
$Fe^{2+} + 4H_2O = Fe^{II}(OH)_4{}^{2-} + 4H^+$	−45.988
$Fe^{3+} + H_2O = Fe^{III}OH^{2+} + H^+$	−2.187
$Fe^{3+} + 2H_2O = Fe^{III}(OH)_2{}^+ + 2H^+$	−4.594
$Fe^{3+} + 3H_2O = Fe^{III}(OH)_3{}^0 + 3H^+$	−13.600
$Fe^{3+} + 4H_2O = Fe^{III}(OH)_4{}^- + 4H^+$	−21.588
$2Fe^{3+} + 2H_2O = Fe^{III}{}_2(OH)_2{}^{4+} + 2H^+$	−2.854
$3Fe^{3+} + 4H_2O = Fe^{III}{}_3(OH)_4{}^{5+} + 4H^+$	−6.288
Solubility product constants	
$Fe^{2+} + 2H_2O = Fe^{II}(OH)_2$(s,amorphous) + $2H^+$	−12.844[c]
$Fe^{3+} + 3H_2O = Fe^{III}(OH)_3$(s,amorphous) + $3H^+$	−3.00[d]

[a] Corrected to zero ionic strength using the Davies equation (Stumm and Morgan, 1996).
[b] Martell et al. (2004).
[c] Cornell and Schwertmann (1996).
[d] Stumm and Morgan (1996).

Table 3
Stability constants[a] for Fe^{II} and Fe^{III} complexes with malonate and oxalate

Equilibrium expression	Log K
Malonate	
$H^+ + L^{2-} = HL^-$	5.696
$2H^+ + L^{2-} = H_2L^0$	8.543
$Fe^{2+} + L^{2-} = Fe^{II}L^0$	2.985
$Fe^{2+} + 2\,L^{2-} = Fe^{II}L_2{}^{2-}$	4.025
$Fe^{3+} + L^{2-} = Fe^{III}L^+$	9.136
$Fe^{3+} + 2L^{2-} = Fe^{III}L_2{}^-$	15.444
$Fe^{3+} + 3L^{2-} = Fe^{III}L_3{}^{3-}$	18.82
Oxalate	
$H^+ + L^{2-} = HL^-$	4.266
$2H^+ + L^{2-} = H_2L^0$	5.518
$Fe^{2+} + L^{2-} = Fe^{II}L^0$	3.865
$Fe^{2+} + 2L^{2-} = Fe^{II}L_2{}^{2-}$	5.895
$Fe^{2+} + 3L^{2-} = Fe^{II}L_3{}^{4-}$	5.220[b]
$Fe^{3+} + L^{2-} = Fe^{III}L^+$	8.803
$Fe^{3+} + 2L^{2-} = Fe^{III}L_2{}^-$	15.441
$Fe^{3+} + 3L^{2-} = Fe^{III}L_3{}^{3-}$	19.823

[a] Martell et al. (2004), unless otherwise noted. Values have been corrected to zero ionic strength using the Davies equation (Stumm and Morgan, 1996).
[b] Schaap et al. (1954).

$$E = E^0 + \frac{RT}{2F}\ln\left(\frac{\{Z^0\}\{H^+\}^2}{\{XH_2{}^0\}}\right), \tag{4}$$

where E^0 is the standard reduction potential for Eq. (2), R is the gas constant (8.314 J K^{-1} mol^{-1}), T is the absolute temperature, and F is the Faraday constant (9.6485×10^4 C mol^{-1}). Both E and E^0 are directly tied to the partial molar Gibbs free energy values (i.e., μ_i^0) (Stumm and Morgan, 1996) and hence the activities of the species in Eq. (2). Since Z^0 and $XH_2{}^0$ are neutral, their activity coefficients are equal to 1.0:

$$E = E^0 + \frac{RT}{2F}\ln(\gamma_+\gamma_+) + \frac{RT}{2F}\ln\left(\frac{[Z^0][H^+]^2}{[XH_2{}^0]}\right). \tag{5}$$

Unfortunately, many reports of standard reduction potentials for organic species fail to provide sufficient information about the medium composition, especially the ionic strength, that allows activity coefficients to be calculated (Clark, 1960). When this situation is encountered, the first two terms in Eq. (5) must be lumped together:

$$E_0 = E^0 + \frac{RT}{2F}\ln(\gamma_+\gamma_+). \tag{6}$$

Hence, Eq. (5) can be rewritten as the following:

$$E = E_0 + \frac{RT}{2F}\ln\left(\frac{[Z^0][H^+]^2}{[XH_2{}^0]}\right). \tag{7}$$

Table 1 makes a distinction between standard reduction potentials for which reliable activity corrections can be made (E^0) and standard reduction potentials that have values that can be expected to vary in unknown ways as the medium composition is changed (E_0) (Clark, 1960). For the reaction presented in Eq. (2), the discrepancy between E^0 and E_0 is −0.001 V at an ionic strength of 1.0×10^{-3} M, and −0.010 V at an ionic strength of 0.50 M. Hence, reduction potential values calculated using E_0 are not far off from values achievable if E^0 values were available.

In order to account for the protonation and deprotonation of $XH_2{}^0$, we write a mass balance equation for the fully reduced form:

$$X_T = [XH_2{}^0] + [XH^-] + [X^{2-}]. \tag{8}$$

Since ${}^cK_{a1} = \frac{[XH^-][H^+]}{[XH_2{}^0]}$ and ${}^cK_{a2} = \frac{[X^{2-}][H^+]}{[XH^-]}$, Eq. (8) becomes the following:

$$X_T = [XH_2{}^0] + \frac{{}^cK_{a1}[XH_2{}^0]}{[H^+]} + \frac{{}^cK_{a1}{}^cK_{a2}[XH_2{}^0]}{[H^+]^2}. \tag{9}$$

Rearrangement of Eq. (9) yields Eq. (10):

$$[XH_2{}^0] = \frac{[H^+]^2 X_T}{[H^+]^2 + {}^cK_{a1}[H^+] + {}^cK_{a1}{}^cK_{a2}}. \tag{10}$$

Substitution of Eq. (10) into Eq. (7) yields Eq. (11):

$$E = E_0 + \frac{RT}{2F} \times \ln\left(\frac{[Z^0]\left([H^+]^2 + {}^cK_{a1}[H^+] + {}^cK_{a1}{}^cK_{a2}\right)}{X_T}\right). \tag{11}$$

For known Z_T ($Z_T = Z^0$) and X_T, the reduction potential (E) at a given pH can be determined using Eq. (11). Essential thermodynamic equations for quinones without Lewis base side-groups are summarized in electronic annex EA-1.

Fig. 2 presents E (in volts) versus pH for the *o*-benzoquinone/catechol and *p*-benzoquinone/hydroquinone half-reactions. For both catechol and hydroquinone, $XH_2{}^0$ is

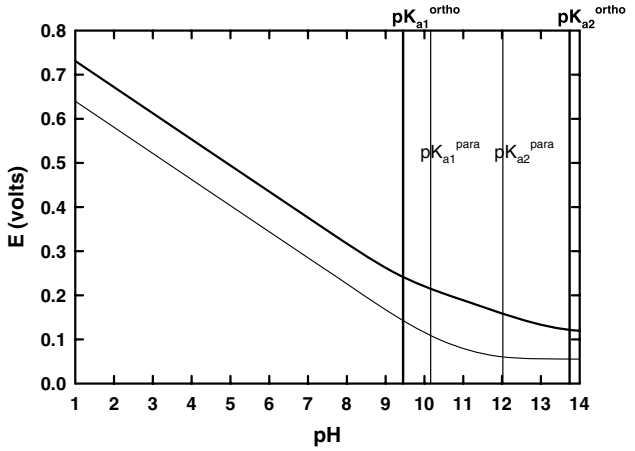

Fig. 2. Two-electron reduction potentials as a function of pH for *p*-benzoquinone/hydroquinone (thin line) and *o*-benzoquinone/catechol (thick line). Calculation conditions: 25 μM Z_T, 25 μM X_T. Vertical lines represent pK_{a1} and pK_{a2} of hydroquinone (thin line) and catechol (thick line).

the predominant protonation level under acidic conditions, which shifts to the species XH^- in the pH range between pK_{a1} and pK_{a2}, and finally to X^{2-} at pH values greater than pK_{a2}. The observed shift in protonation level of the reduced species, in turn, affects the slope of the E versus pH plot, as described below.

To assess the pH effects on reduction potential, we start by expressing Eq. (11) in terms of $\log_{10}$:

$$E = E_0 + \frac{2.303\ RT}{2F}\log\left(\frac{[Z^0]}{X_T}\right) + \frac{2.303\ RT}{2F} \times \log\left([H^+]^2 + {}^cK_{a1}[H^+] + {}^cK_{a1}{}^cK_{a2}\right). \quad (12)$$

Using the relationship $pH = -\log[H^+]$, slopes in Fig. 2 can be quantitatively justified:

Below pK_{a1}: $[H^+]^2 \gg ({}^cK_{a1}[H^+] + {}^cK_{a1}{}^cK_{a2})$

$$E \cong E_0 + \frac{2.303\ RT}{2F}\log\left(\frac{[Z^0]}{X_T}\right) - \frac{2.303\ RT}{F}\ (pH) \quad (13)$$

$$= E_0 + \frac{2.303\ RT}{2F}\log\left(\frac{[Z^0]}{X_T}\right) - 0.059\ (pH). \quad (14)$$

Between pK_{a1} and pK_{a2}: ${}^cK_{a1}[H^+] \gg \left([H^+]^2 + {}^cK_{a1}{}^cK_{a2}\right)$

$$E \cong E_0 + \frac{2.303\ RT}{2F}\log\left(\frac{[Z^0]}{X_T}\right) + \frac{2.303\ RT}{2F}\log {}^cK_{a1} - \frac{2.303\ RT}{2F}\ (pH) \quad (15)$$

$$= E_0 + \frac{2.303\ RT}{2F}\log\left(\frac{[Z^0]}{X_T}\right) + \frac{2.303\ RT}{2F}\log {}^cK_{a1} - 0.030\ (pH). \quad (16)$$

Above pK_{a2}: ${}^cK_{a1}{}^cK_{a2} \gg \left([H^+]^2 + {}^cK_{a1}[H^+]\right)$

$$E \cong E_0 + \frac{2.303\ RT}{2F}\log\left(\frac{[Z^0]}{X_T}\right) + \frac{2.303\ RT}{2F} \times \log {}^cK_{a1}{}^cK_{a2}. \quad (17)$$

Inspection of Eqs. (14), (16), and (17) indicate that slopes for plots of E change from −0.059 to −0.030, and finally to 0.0 as the pH reaches pK_{a1} and pK_{a2}. Fig. 2 indicates that the reduction potential of the *o*-benzoquinone system is approximately 0.1 V higher than that of the *p*-benzoquinone system, and that the catechol monoanion (XH^-, predominant between pK_{a1} and pK_{a2}) is stable over a wider pH range than the hydroquinone monoanion.

Fig. 3 presents plots of E versus pH for chloro- and 2,5-dimethyl-substituted *p*-benzoquinone/hydroquinone redox couples. Added ring substituents yielded E versus pH plots with the general features described above for the unsubstituted form, albeit with line shifts. As shown in Fig. 3, dimethyl substitution lowers E at a fixed pH, reflecting greater stability of the fully oxidized benzoquinone form relative to the fully reduced hydroquinone form. Both pK_{a1} and pK_{a2} of the fully reduced form are raised, and as a consequence the eventual leveling out of the E versus pH line occurs at higher pH. Both observations are the consequences of a electron-donating effect of the dimethyl substituent, which compensate for the electron deficit experienced by the aromatic ring during oxidation and protonation (Bruice, 1998). Because of its electron-withdrawing nature, chloro substituent yields opposite effects (Fig. 3).

Inductive and resonance effects of ring substituents are the primary contributing factors to the overall electronic characteristics of a given quinone molecule:

(i) Inductive effects (Bruice, 1998): sigma electron-donating substituents, such as –CH_3, raise the pK_a of the fully reduced form $XH_2{}^0$ and lower E^0 for the half-reaction shown in Eq. (2). Sigma electron-withdrawing substituents, such as –$NH_3{}^+$, yield the opposite effect.

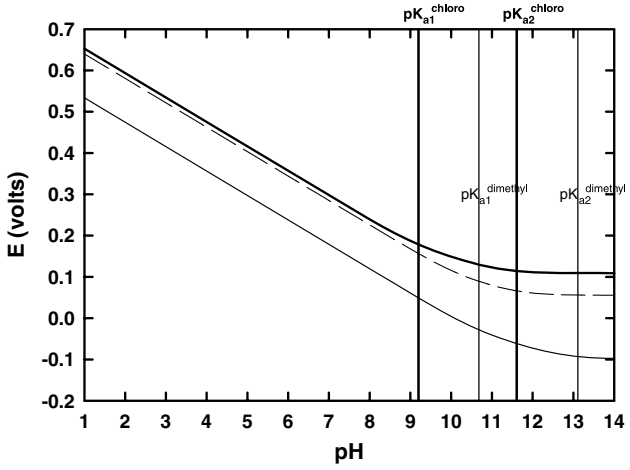

Fig. 3. Effects of chloro (thick solid line) and 2,5-dimethyl (thin solid line) substituents on the two-electron reduction potential of *p*-benzoquinone/hydroquinone. A dashed line for the unsubstituted couple is also shown for a reference. Calculation conditions: 25 μM Z_T, 25 μM X_T. Vertical lines represent pK_{a1} and pK_{a2} of chloro- (thick line) and 2,5-dimethyl- (thin line) substituted hydroquinones.

(ii) Resonance effects (Bruice, 1998) arise from the stabilization that accompanies the delocalization of electrons within a molecular structure. Substituents possessing a pair of non-bonded electrons on the atom directly attached to the ring (e.g., –OH) are able to donate electrons by resonance. Substituents such as $–NO_2$, $–SO_3H$, –COOH, and –COR withdraw electrons by resonance delocalization of π electrons of the aromatic ring onto the substituent (Bruice, 1998). As aromatic ring numbers increase from benzene to naphthalene to anthracene, greater resonance stabilization within the fully reduced form XH_2^0 causes a decrease in $E^0(Z^0/XH_2^0)$ values.

3.2. Quinones with Lewis base side-groups

Based upon potentiometric titrations (Ritchie and Perdue, 2003) and NMR (Thorn et al., 1992) studies, most investigators believe that aromatic –COOH and –OH groups are the most abundant Lewis base groups within NOM. Although specific NOM structures are yet to be characterized, natural products such as caffeic acid (Deiana et al., 1995), gentisic acid (Capelle et al., 1996), and juglone (Schwarzenbach et al., 1990) can serve as illustrative examples.

The pH dependence of each benzoquinone/dihydroxybenzene half-reaction is influenced by the pK_a values of the Lewis base side-groups (–R) of both fully oxidized and fully reduced oxidation states:

$$H_2X\text{-}RH^0 = H_2X\text{-}R^- + H^+ \quad pK_{aR} \tag{18}$$

$$H_2X\text{-}R^- = HX^-\text{-}R^- + H^+ \quad pK_{a1} \tag{19}$$

$$HX^-\text{-}R^- = X^{2-}\text{-}R^- + H^+ \quad pK_{a2} \tag{20}$$

$$Z\text{-}RH^0 = Z\text{-}R^- + H^+ \quad pK_{aZ} \tag{21}$$

Differences in Lewis base pK_a values between the fully reduced (Eqs. (18)–(20)) and the fully oxidized (Eq. (21)) forms matter the most to the energetics of two-electron oxidation. Fig. 4 presents plots of E versus pH for benzoquinoneacetic acid/homogentisic acid redox couple. Lewis base side-group on benzoquinoneacetic acid possess following pK_a values: $pK_{aR} = 4.30$, $pK_{aZ} = 3.30$ (Table 1). The carboxylic acid/carboxylate group is electronically isolated from the ring by the methylene group. Indeed, the methylene group makes the $–CH_2COOH/–CH_2COO^-$ substituent net electron-donating. As a consequence, E for the benzoquinoneacetic acid/homogentisic acid half-reaction is lower than that for *p*-benzoquinone/hydroquinone. Unlike in Fig. 3, lines in Fig. 4 are not parallel to one another. In fact, the slope of benzoquinoneacetic acid/homogentisic acid couple increases after passing pK_{aZ}, and further increases past pK_{aR} (Fig. 4). Deprotonation of the ring substituent with increasing pH makes it more electron-donating and further stabilizes the benzoquinone form.

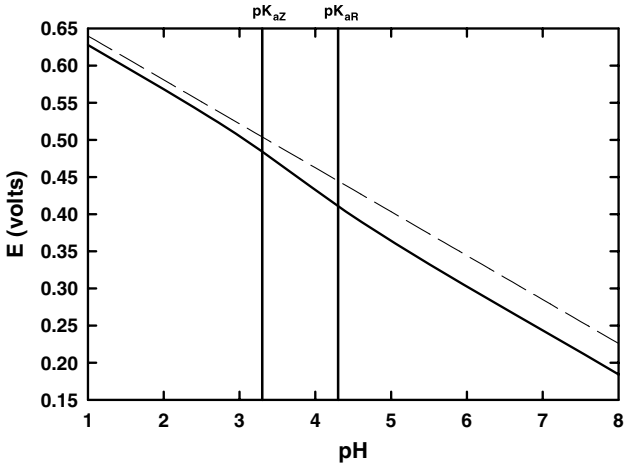

Fig. 4. Plots of E versus pH for benzoquinoneacetic acid/homogentisic acid redox couple (thick line). Calculation conditions: 25 μM Z_T and 25 μM X_T. Vertical lines represent pK_{aZ} and pK_R. Thin line for *p*-benzoquinone/hydroquinone redox couple is shown for a reference.

3.3. Semiquinone radicals

Semiquinone radicals are formed from the one-electron oxidation of dihydroxybenzenes, from the one-electron reduction of benzoquinones, or from one-electron transfer from dihydroxybenzenes to benzoquinones, in a process termed comproportionation (Roginsky et al., 1999), as summarized in Fig. 1. From the acid–base reaction described in Fig. 1, following mass balance for the semiquinone radical (Y_T) can be obtained:

$$Y_T = [Y^{\cdot -}] + [HY^{\cdot -}]. \tag{22}$$

Mass balance and electron balance equations are needed to quantify Y_T arising from comproportionation at fixed X_T and Z_T. The mass balance for a quinone system (S_T) can be written as shown below.

$$S_T = X_T + Y_T + Z_T, \tag{23}$$

$$S_T = [XH_2^0] + [XH^-] + [X^{2-}] + [YH^{\cdot}] + [Y^{\cdot -}] + [Z^0]. \tag{24}$$

To establish an electron balance, it is useful to classify different oxidation states in terms of the "electron levels". Two-electron and one-electron quinone half-reactions shown in Fig. 1 (Equations F1-1, F1-4, and F1-6) provide the basis for assigning the electron levels: a level of 2 for dihydroxybenzenes, a level of 1 for semiquinone radicals, and a level of 0 for benzoquinones. These electron levels, in turn, allow us to write a mass balance equation for electrons:

$$e_T = 2X_{T,t=0} + Y_{T,t=0} = 2X_{T,eq} + Y_{T,eq}, \tag{25}$$

$$e_T = 2[XH_2^0] + 2[XH^-] + 2[X^{2-}] + [YH^{\cdot}] + [Y^{\cdot -}]. \tag{26}$$

Concentrations for all quinone species can be written in terms of $[Z^0]$, as shown in electronic annex EA-2. The following equation provides the electron balance equation rewritten in terms of $[Z^0]$:

$$e_T = 2\mathrm{EXP}\left(-\frac{2F(E-E^0_{ZX})}{RT}\right)\left(\frac{[H^+]^2}{K_{a1}K_{a2}}+\frac{[H^+]}{K_{a2}}+1\right)[Z^0] + \mathrm{EXP}\left(-\frac{F(E-E^0_{ZY})}{RT}\right)\left(\frac{[H^+]}{K_{aY}}+1\right)[Z^0]. \quad (27)$$

Likewise, mass balance equation can be rewritten in terms of $[Z^0]$:

$$S_T = \mathrm{EXP}\left(-\frac{2F}{RT}(E-E^0_{ZX})\right)\left(\frac{[H^+]^2}{K_{a1}K_{a2}}+\frac{[H^+]}{K_{a2}}+1\right)[Z^0] + \mathrm{EXP}\left(-\frac{F}{RT}(E-E^0_{ZY})\right)\left(\frac{[H^+]}{K_{aY}}+1\right)[Z^0] + [Z^0]. \quad (28)$$

At equilibrium, E is the same for all half reactions considered. Mass balance for quinones (S_T; Eq. (28)) and electrons (e_T; Eq. (27)) constitute two equations with two unknowns (E, $[Z^0]$). For known S_T and e_T, two unknowns, E and $[Z^0]$, can be determined by iteration. Subsequently, concentrations of semiquinone radical species can be determined using EA-2.

Fig. 5 presents plots of $\log[YH^\cdot]$, $\log[Y^{\cdot-}]$, and $\log(Y_T)$ as a function of pH at fixed X_T (25 μM) and Z_T (25 μM) for unsubstituted *ortho*- and *para*-quinone systems. Recall that XH_2^0 and Z^0 are the predominant protonation levels of the fully reduced and fully oxidized forms within the pH range shown. The linear increase in $\log[Y^{\cdot-}]$ with increasing pH is a direct consequence of the following reaction:

$$Z^0 + XH_2^0 = 2Y^{\cdot-} + 2H^+ \quad (29)$$

The observation that $\log[YH^\cdot]$ is independent of pH is the consequence of reaction provided in Equation F1-7 in Fig. 1. The net effect is that comproportionation is largely independent of pH below the pK_{aY} of the semiquinone radical, but grows in importance with increasing pH once the pH is greater than the pK_{aY}.

The *ortho*-quinone system possesses higher K_{com} value of 10^{-12} than the *para*-quinone system (10^{-13}; Fig. 1). Fig. 5 nicely illustrates the dual role of K_{com} and pK_{aY} in setting Y_T. Under strongly acidic conditions, Y_T is 25-times lower for the *para*-quinone system, a direct consequence of the lower value of K_{com} relative to that of the *ortho*-quinone system. As the pH is increased, the pK_{aY} for the *para*-radical is reached 0.9 log units earlier than for the *ortho*-radical. For this reason, Y_T under neutral and alkaline conditions is only 3-times lower for the *para*-quinone system than the *ortho*-quinone system.

3.4. Iron speciation in non-complexing electrolytes and in the presence of ligands

For Fe^{II} in simple electrolyte media without added ligands, the following equation represents the total dissolved Fe^{II} concentration ($Fe^{II}{}_T$).

$$Fe^{II}{}_T = [Fe_{(aq)}{}^{2+}] + [Fe^{II}OH^+] + [Fe^{II}(OH)_2{}^0] + [Fe^{II}(OH)_3{}^-] + [Fe^{II}(OH)_4{}^{2-}]. \quad (30)$$

The concentration of each dissolved species within $Fe^{II}{}_T$ is set by its complex formation constant (K), as shown in electronic annex EA-3. Electronic annex EA-4 provides ways to express all Fe^{II} species in terms of $Fe_{(aq)}{}^{2+}$ concentration, allowing us to rewrite Eq. (30) in terms of $[Fe_{(aq)}{}^{2+}]$. Whenever a solubility-limiting solid-phase such as $Fe^{II}(OH)_2$(s,amorph) exists in a system, $[Fe_{(aq)}{}^{2+}]$ is fixed by the solubility product constant (K_{SO}). Using EA-4, analogous procedure should be followed to determine Fe^{III} speciation.

When iron-coordinating organic ligands are present, a mass balance equation for the total dissolved ligand (L_T) must be established (electronic annex EA-5). An example

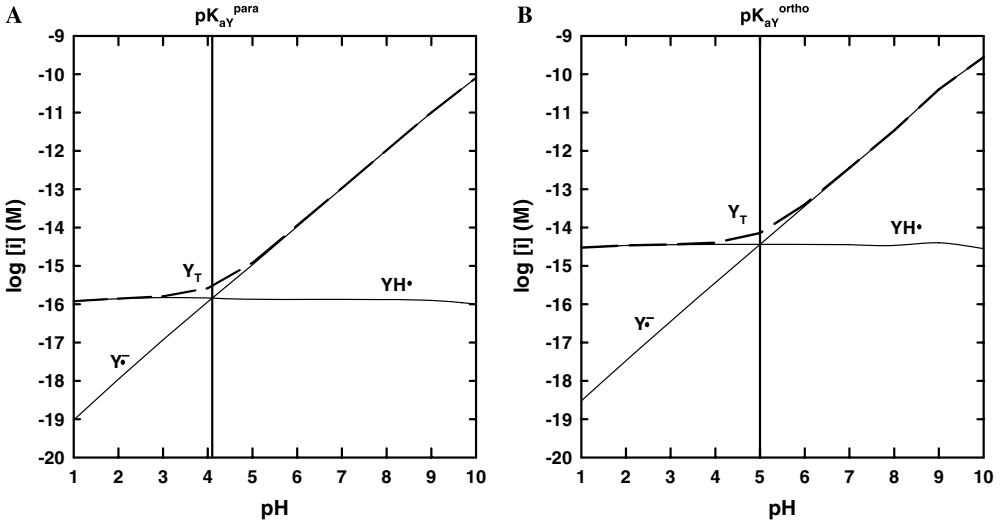

Fig. 5. Total concentrations and protonation levels for semiquinone radicals achieved by equilibrium comproportionation reactions in systems consisting of (A) hydroquinone and *p*-benzoquinone and (B) catechol and *o*-benzoquinone. For each calculation, $X_T = Z_T = 25$ μM.

is given below for Fe^{II} in the presence of dicarboxylate chelating agent oxalate.

$$L_T = [H_2L^0] + [HL^-] + [L^{2-}] + [Fe^{II}L^0] + 2[Fe^{II}L_2^{2-}] + 3[Fe^{II}L_3^{4-}]. \quad (31)$$

For $Fe^{II}{}_T$, additional terms for Fe^{II}–oxalate complexes are needed, as shown in bold below:

$$Fe_T{}^{II} = [Fe_{(aq)}{}^{2+}] + [Fe^{II}OH^+] + [Fe^{II}(OH)_2{}^0] + [Fe^{II}(OH)_3{}^-] + [Fe^{II}(OH)_4{}^{2-}] + [\mathbf{Fe^{II}L^0}] + [\mathbf{Fe^{II}L_2{}^{2-}}] + [\mathbf{Fe^{II}L_3{}^{4-}}]. \quad (32)$$

The concentration of each species in Eqs. (31) and (32) can be related back to free iron ($[Fe^{2+}]$) and free oxalate ($[L^{2-}]$) concentrations using the corresponding equilibrium constant (K), as shown in electronic annex EA-6. When $Fe^{II}{}_T$ and L_T are known, Eqs. (31) and (32) provide solutions for the two unknowns, $[L^{2-}]$ and $[Fe^{2+}]$. Similar procedure should be followed to determine Fe^{III} speciation in the presence of iron-coordinating organic ligands using EA-5.

Fig. 6 shows the speciation of Fe^{II} and Fe^{III} as a function of pH in the presence of a 10-fold excess of oxalate. At low pH, metal ions must compete with protons for available chelating agent. The higher charge and smaller radius of Fe^{III} cause it to be more successful than Fe^{II} at capturing chelating agents under acidic conditions. Indeed, complexation by Fe^{III} exceeds complexation by Fe^{II} as the pH is increased until the point is reached where $Fe^{III}(OH)_3$ (s,amorphous) precipitates. Above pH 6.0, complexation with Fe^{III} drops off considerably; free chelating agent is unable to compete successfully with hydroxide ion for available Fe^{III}. As noted earlier, Fe^{II} exhibits a much lower affinity for hydroxide ion, and this is reflected in the speciation calculations: the highest concentrations of total complexed Fe^{II} appear at higher pH than for Fe^{III} complexes. For both Fe^{III} and Fe^{II}, the greatest complex formation with oxalate is achieved at pH range where the protonation of organic ligand and the hydrolysis of iron are least significant. Analogous iron speciation diagram in the presence of excess malonate is provided in electronic annex EA-7.

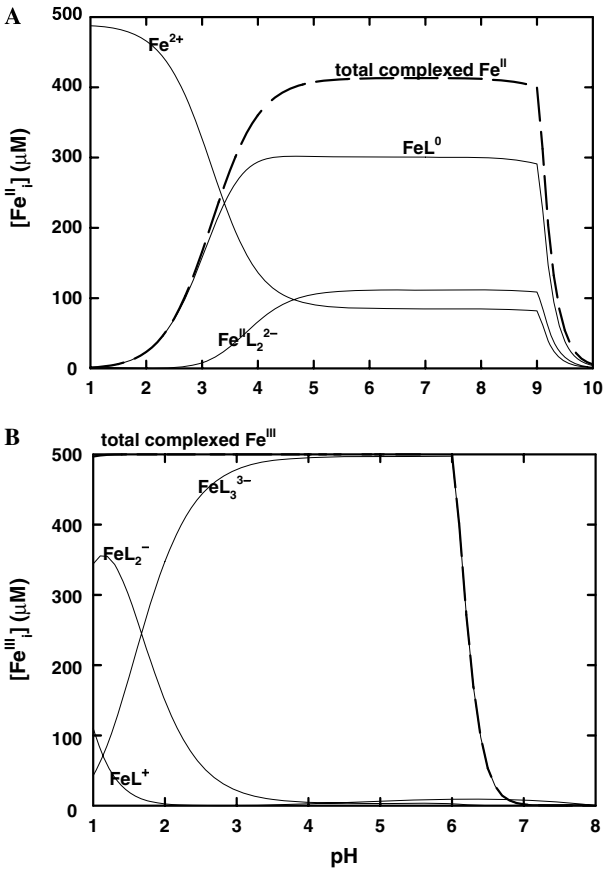

Fig. 6. Effect of 5 mM oxalate on the speciation of (A) 500 μM $TOTFe^{II}$ and (B) 500 μM $TOTFe^{III}$ as a function of pH. $Fe(OH)_2$(s,amorphous) and $Fe(OH)_3$(s,amorphous) are used as the solubility-limiting phases.

We now turn our attention to the calculation of reduction potential for systems containing both Fe^{II} and Fe^{III}. The first step is to separately work out the acid–base speciation of the two oxidation states using mass balance equations. Calculated values for $[Fe_{(aq)}{}^{2+}]$ and $[Fe_{(aq)}{}^{3+}]$ are then inserted into the Nernst equation shown in Eq. (34).

$$Fe^{3+} + e^- = Fe^{2+} \quad E_0(Fe^{3+}/Fe^{2+}) = 0.776\,V, \quad (33)$$

$$E(Fe^{III}/Fe^{II}) = E_0 + \frac{RT}{F}\ln\frac{[Fe^{3+}]}{[Fe^{2+}]}. \quad (34)$$

As shown in Fig. 7, the effect of increasing oxalate and malonate concentrations on E versus pH plots is complex. It is useful to start by noting the lowest pH where $Fe^{III}(OH)_3$(s) precipitation takes place. Increasing the chelating agent concentration raises the pH of precipitation, and oxalate yields a higher pH of precipitation than an equal concentration of malonate. When the pH is below the point where $Fe^{III}(OH)_3$(s) precipitation takes place, adding chelating agent causes both $[Fe_{(aq)}{}^{2+}]$ and $[Fe_{(aq)}{}^{3+}]$ to decrease. The decrease in $[Fe_{(aq)}{}^{3+}]$ is greater, however, because of the greater affinity of oxalate and malonate for the oxidation state with the higher charge and smaller radius. In agreement with Eq. (34), a lowering of the reduction potential with increasing chelating agent concentration is observed.

When the pH is above the point where $Fe^{III}(OH)_3$(s) precipitation takes place, $[Fe_{(aq)}{}^{3+}]$ is "fixed" by the solubility product constant (Table 2) and therefore is independent of the chelating agent concentration. $[Fe_{(aq)}{}^{2+}]$, however, decreases with increasing chelating agent concentration, since there is no "reservoir" of solid-phase Fe^{II} to draw from. In agreement with Eq. (34), a rise in reduction potential with increasing chelating agent concentration is observed.

When the pH is above the point where $Fe^{II}(OH)_2$(s) precipitation takes place in addition to $Fe^{III}(OH)_3$(s), both $[Fe_{(aq)}{}^{2+}]$ and $[Fe_{(aq)}{}^{3+}]$ are "fixed" by the solubility product constants (Table 2). In agreement with Eq. (34), chelating agent concentration no longer influences the iron reduction potential. For a detailed description of iron speciation in the presence of additional organic acids citric

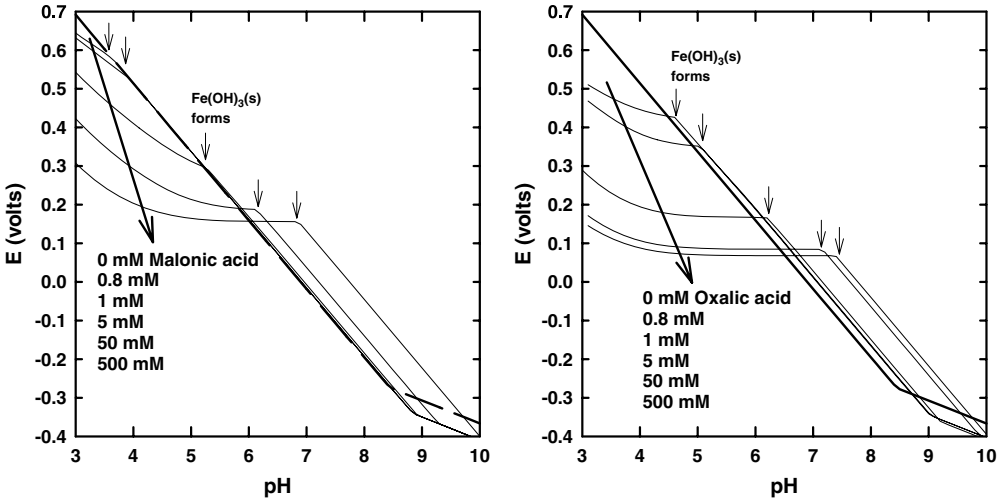

Fig. 7. Effect of increasing oxalate and malonate concentrations on the reduction potential of iron. In each figure, both $TOTFe^{II}$ and $TOTFe^{III}$ were fixed at 250 μM (TOTFe = 500 μM). $Fe^{II}(OH)_2$(s,amorphous) and $Fe^{III}(OH)_3$(s,amorphous) were used as solubility-limiting phases. Arrows indicate the pH where $Fe^{III}(OH)_3$(s) first begins to form.

acid and mugineic acid, readers are referred to a review by Stone (1997).

4. Chemical reactions

4.1. Cross reactions between quinones

In a process termed cross reaction, quinone species with one structure (System I) engage in electron transfer reactions with quinone species having a different structure (System II). Mass balance equations for quinones and electron are needed to determine quinone speciation as a result of cross reaction. To keep the two systems distinct, the nomenclature used to denote three different oxidation states of the first quinone system (X, Y, and Z) needs to be expanded to deal with a second quinone system. The symbols A, B, and C will be used to denote the fully oxidized, intermediate, and fully reduced oxidation states of the second quinone system:

System I	System II		Electron level
Dihydroxybenzene:			
X_T (Eq. (8))	$A_T = [AH_2^0] + [AH^-] + [A^{2-}]$	(35)	2
Semiquinone radical:			
Y_T (Eq. (22))	$B_T = [BH^{\cdot}] + [B^{-}]$	(36)	1
Benzoquinone:			
Z_T	$C_T = [C^0]$	(37)	0

The assigned electron levels allow us to write a mass balance equation for electrons:

$$\begin{aligned} e_T &= 2X_{T,t=0} + 2A_{T,t=0} + Y_{T,t=0} + B_{T,t=0} \\ &= 2X_{T,eq} + 2A_{T,eq} + Y_{T,eq} + B_{T,eq}, \end{aligned} \tag{38}$$

$$\begin{aligned} e_T = {} & 2[XH_2^0] + 2[XH^-] + 2[X^{2-}] + 2[AH_2^0] + 2[AH^-] \\ & + 2[A^{2-}] + [YH^{\cdot}] + [Y^{\cdot-}] + [BH^{\cdot}] + [B^{\cdot-}]. \end{aligned} \tag{39}$$

EA-2 shows how to write concentrations for all quinone species in terms of $[Z^0]$ and $[C^0]$, which enables us to rewrite Eq. (39) as the following:

$$\begin{aligned} e_T = {} & 2\mathrm{EXP}\left(-\frac{2F(E-E^0_{XZ})}{RT}\right)\left(\frac{[H^+]^2}{K_{aX1}K_{aX2}}+\frac{[H^+]}{K_{aX2}}+1\right)[Z^0] \\ & + \mathrm{EXP}\left(-\frac{F(E-E^0_{YZ})}{RT}\right)\left(\frac{[H^+]}{K_{aY}}+1\right)[Z^0] \\ & + 2\mathrm{EXP}\left(-\frac{2F(E-E^0_{AC})}{RT}\right)\left(\frac{[H^+]^2}{K_{aA1}K_{aA2}}+\frac{[H^+]}{K_{aA2}}+1\right)[C^0] \\ & + \mathrm{EXP}\left(-\frac{F(E-E^0_{BC})}{RT}\right)\left(\frac{[H^+]}{K_{aB}}+1\right)[C^0]. \end{aligned} \tag{40}$$

In Eq. (28), mass balance equations for the quinone System I was expressed in terms of $[Z^0]$. Following the procedure described for obtaining Eq. (28), mass balance equation for the second quinone system can be expressed in terms of $[C^0]$.

At equilibrium, E is the same for all half reactions considered. Mass balance equations for electrons and the two quinones systems constitute three equations with three unknowns (E, $[Z^0]$, and $[C^0]$). After solving for unknowns by iteration, concentration of each quinone species can be calculated as shown in electronic annex EA-2.

As an illustrative example, consider the following initial conditions (case (i)): 100 μM XH_2 and 100 μM C^0. Using Eq. (38), the following electron balance holds:

$$\begin{aligned} 2[X_T]_{t=0} &= 200\ \mu M \\ &= 2X_{T,eq} + 2A_{T,eq} + Y_{T,eq} + B_{T,eq}. \end{aligned} \tag{41}$$

The quinone mass balance equals to 200 μM.

Now consider different initial conditions (case (ii)): 50 μM XH_2, 50 μM Z^0, 50 μM AH_2, and 50 μM C^0. The following electron balance holds:

$$2[X_T]_{t=0} + 2[A_T]_{t=0} = 200\ \mu M = 2X_{T,eq} + 2A_{T,eq} + Y_{T,eq} + B_{T,eq}. \quad (42)$$

Like in case (i), the quinone mass balance in case (ii) equals to 200 μM. Therefore, case (i) and case (ii) afford the same electron balance (200 μM) and quinone mass balance (200 μM). We will use the concentration of hydroquinone formed (X_T) as a measure of reaction progress when equilibrium is attained. Since the set of equations and inputted parameters for the two cases are the same, both cases yields the same X_T.

In Fig. 8, *p*-benzoquinone (System I) is reacted separately with three different reductants (System II), chlorohydroquinone, 2,5-dimethylhydroquinone, and homogentisic acid. As shown in Fig. 3, *E* (hydroquinone/benzoquinone) and *E*(chlorohydroquinone/chlorobenzoquinone) decrease with increasing pH, but the slopes of the two plots are the same up to pH approximately 9.0. As a consequence, X_T does not change with pH when *p*-benzoquinone is reacted with chlorohydroquinone (Fig. 8). Similar pH dependence observed for the dimethyl-substituted quinone in Fig. 3 resulted in the negligible pH effects on X_T when 2,5-dimethylhydroquinone is the reductant (Fig. 8).

As discussed previously (Fig. 4), protonation/deprotonation of the $-CH_2COOH$ side-group alters the pH dependence of the benzoquinoneacetic acid/homogentisic acid half-reaction. As a consequence, using this quinone system in a cross reaction with *p*-benzoquinone/hydroquinone (Fig. 8) yields a shift in product yield in the vicinity of its pK_{aR} and pK_{aZ} (Table 1). Deprotonation of ring substituent near pK_{aZ} and pK_{aR} decreases *E* (benzoquinoneacetic acid/homogentisic acid), while *E* (hydroquinone/benzoquinone) is relatively insensitive to pH (Fig. 4). The lower *E* of the reductant half-reaction results in higher driving force for the reduction of *p*-benzoquinone, thus affording greater X_T at higher pH (Fig. 8).

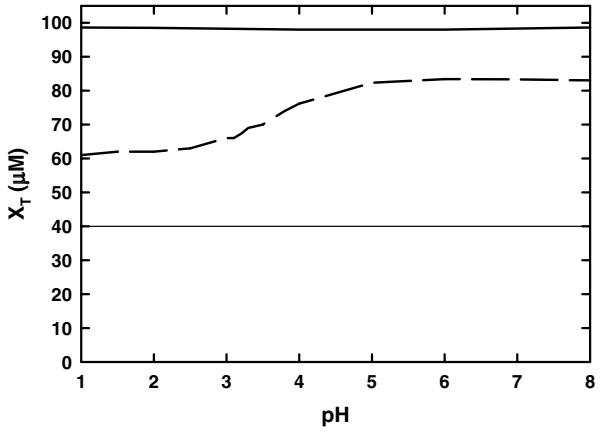

Fig. 8. Hundred micromolar of *p*-benzoquinone undergoes cross reaction with 100 μM chlorohydroquinone (thin solid line), 2,5-dimethylhydroquinone (thick solid line), and homogentisic acid (thick dashed line) until equilibrium conditions are attained. The *y*-axis shows the hydroquinone concentration attained at equilibrium.

Fig. 8 also illustrates the influence of ring substituents on X_T at a fixed pH. A stronger reductant, possessing a lower $E_0(Z^0/XH_2)$, yields a higher X_T. Throughout the pH range of reaction in Fig. 8, the extent of reaction increases in the following order: chlorohydroquinone (0.712 V), homogentisic acid (0.687 V), and 2,5-dimethylhydroquinone (0.593 V).

4.2. Iron in non-complexing media and quinones

When the reaction is fully reversible, dihydroxybenzenes (XH_2) can reduce Fe^{III}, while corresponding benzoquinones (Z^0) can oxidize Fe^{II} (Eq. (1)). Electron and mass balance equations for the quinone system have been described in the previous section. From the Nernst equation for iron described in Eq. (34), the electron level of Fe^{II} equals to one, and the electron level of Fe^{III} equals to zero. From electron levels for quinone and iron, a net mass balance equation for electrons can be written:

$$e_T = 2X_{T,t=0} + Y_{T,t=0} + Fe^{II}_{T,t=0} = 2X_{T,eq} + Y_{T,eq} + Fe^{II}_{T,eq}, \quad (43)$$

$$e_T = 2[XH_2^{\,0}] + 2[XH^-] + 2[X^{2-}] + [YH^{\cdot}] + [Y^{\cdot -}] + [Fe^{2+}] + [Fe^{II}OH^+] + Fe^{II}(OH)_2^{\,0}] + [Fe^{II}(OH)_3^{\,-}] + [Fe^{II}(OH)_4^{\,2-}]. \quad (44)$$

As shown in electronic annexes EA-2 and EA-4, Eq. (44) can be rewritten in terms of $[Z^0]$ and $[Fe^{2+}]$.

$$e_T = 2EXP\left(-\frac{2F(E-E^0_{XZ})}{RT}\right)\left(\frac{[H^+]^2}{K_{aX1}K_{aX2}} + \frac{[H^+]}{K_{aX2}} + 1\right)[Z^0] + EXP\left(-\frac{F(E-E^0_{YZ})}{RT}\right)\left(\frac{[H^+]}{K_{aY}} + 1\right)[Z^0] + [Fe^{2+}_{(aq)}] + K_{FeOH^+}[Fe^{2+}_{(aq)}][OH^-] + K_{Fe(OH)_2^{\,0}}[Fe^{2+}_{(aq)}][OH^-]^2 + K_{Fe(OH)_3^{\,-}}[Fe^{2+}_{(aq)}][OH^-]^3 + K_{Fe(OH)_4^{\,2-}}[Fe^{2+}_{(aq)}][OH^-]^4. \quad (45)$$

The mass balance equation for the iron system (Fe_T) is described below.

$$Fe_T = Fe^{II}_T + Fe^{III}_T. \quad (46)$$

As shown in electronic annex EA-4, Eq. (46) can be expressed in terms of $[Fe^{2+}]$:

$$\begin{aligned}Fe_T = {} & [Fe_{(aq)}^{2+}] + K_{FeOH^+}[Fe_{(aq)}^{2+}][OH^-] \\ & + K_{Fe(OH)_2^0}[Fe_{(aq)}^{2+}][OH^-]^2 \\ & + K_{Fe(OH)_3^-}[Fe_{(aq)}^{2+}][OH^-]^3 + K_{Fe(OH)_4^{2-}}[Fe_{(aq)}^{2+}][OH^-]^4 \\ & + EXP\left(\frac{F(E-E^0)}{RT}\right)[Fe^{2+}] \\ & + K_{FeOH^{2+}}EXP\left(\frac{F(E-E^0)}{RT}\right)[Fe^{2+}][OH^-] \\ & + K_{Fe(OH)_2^+}EXP\left(\frac{F(E-E^0)}{RT}\right)[Fe^{2+}][OH^-]^2 \\ & + K_{Fe(OH)_3^0}EXP\left(\frac{F(E-E^0)}{RT}\right)[Fe^{2+}][OH^-]^3 \\ & + K_{Fe(OH)_4^-}EXP\left(\frac{F(E-E^0)}{RT}\right)[Fe^{2+}][OH^-]^4. \end{aligned} \quad (47)$$

For the quinone system, Eq. (28) shows how to express S_T in terms of $[Z^0]$. Mass balance equations for electron (e_T), quinone (S_T) and iron (Fe_T) constitute three equations with three unknowns (E, $[Fe^2(aq)]$, and $[Z^0]$). Speciation of both quinone and iron systems can be determined after solving for the unknowns at a given pH by iteration.

Electronic annexes EA-3 and EA-4 provide different equations for determining iron speciation. We start with the assumption that solubility-limiting phases do not form. The ion activity product for $[Fe^{2+}(aq)]$ with respect to $Fe(OH)_2$(s, am.) and $[Fe^{3+}(aq)]$ with respect to $Fe(OH)_3$ (s,am.) is then calculated. If the solubility has been exceeded, speciation is recalculated with the $[Fe^{2+}(aq)]$ and/or $[Fe^{3+}(aq)]$ fixed using the solubility product constant.

We will use the concentration of hydroquinone formed (X_T) as a measure of reaction progress. As the sigmoidal curves in Fig. 9 indicate, little reaction takes place for any of the quinone systems below pH 3.0, while nearly complete reduction takes place at pH values greater than 9.0. Within the intermediate pH region, reduction is most advanced for the quinone system with the highest value of $E_0(Z^0/XH_2)$ (Table 1). At a fixed pH, the extent of reduction increases from AQDS, juglone, to *p*-benzoquinone.

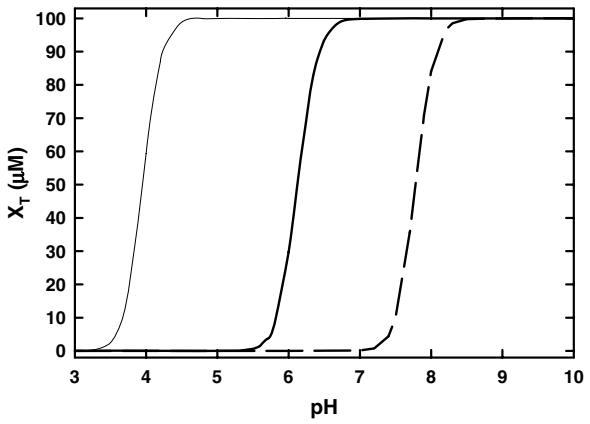

Fig. 9. Reduction of *p*-benzoquinone (thin dashed line), juglone (thick solid line), and AQDS (thick dashed line) with Fe^{II}. Calculation conditions: 100 μM Z_T, 500 μM $TOTFe^{II}$. $Fe^{III}(OH)_3$(s,amorph) and $Fe^{II}(OH)_2$(s,amorph) were used as solubility-limiting phases. The *y*-axis shows the reduced product concentration attained at equilibrium.

Let us suppose that the analytical procedure that we are employing can detect XH_2^0 product concentrations in excess of 0.10 μM. As indicated by Fig. 9, there is a minimum pH needed to achieve this concentration. If the initial Fe^{2+} and Z^0 concentrations are known, and our "analytical criterion" for $[XH_2^0]$ has been set, then the minimum pH needed can be calculated using the expression for calculating Gibbs free energy corresponding to the reaction shown in Eq. (1):

$$\Delta G = \Delta G^0 + RT \quad \ln\left(\frac{a^2_{Fe(OH)3}[XH_2^0][H^+]^4}{[Fe^{2+}]^2[Z^0]}\right). \quad (48)$$

We set ΔG equal to zero and solve for $[H^+]$. When the pH is below the calculated value, the analytical criterion for $[XH_2^0]$ will not be met, and we will not detect appreciable reaction progress. As the pH is increased above this value, the reaction shown in Eq. (1) will progress more and more to the right, until $[XH_2^0]$ reaches a maximum at nearly stoichiometry-limited values.

4.3. Iron in the presence of ligands and quinones

Ways to modify the iron mass balance upon oxalate addition have been described earlier (EA-5 and EA-6). Like for the iron mass balance, additional terms for iron–oxalate complexes are included in the electron balance equation, as written in bold below:

$$\begin{aligned} e_T = {} & 2[XH_2^0] + 2[XH^-] + 2[X^{2-}] + [YH^\cdot] + [Y^{\cdot-}] \\ & + [Fe^{2+}] + [Fe^{II}OH^+] + [Fe^{II}(OH)_2^0] + [Fe^{II}(OH)_3^-] \\ & + [Fe^{II}(OH)_4^{2-}] + \mathbf{[Fe^{II}L^0][Fe^{II}L_2^{2-}][Fe^{II}L_3^{4-}]}. \end{aligned} \quad (49)$$

EA-6 shows ways to write concentrations for all iron species in terms of Fe^{2+} and L^{2-} concentrations in the presence of oxalate. Using EA-2 and EA-6, Eq. (49) can now be rewritten in terms of $[Fe^{2+}]$, $[L^{2-}]$, and $[Z^0]$:

$$\begin{aligned} e_T = {} & 2EXP\left(-\frac{2F(E-E^0_{XZ})}{RT}\right)\left(\frac{[H^+]^2}{K_{aX1}K_{aX2}} + \frac{[H^+]}{K_{aX2}} + 1\right)[Z^0] \\ & + EXP\left(-\frac{F(E-E^0_{YZ})}{RT}\right)\left(\frac{[H^+]}{K_{aY}} + 1\right)[Z^0] \\ & + [Fe_{(aq)}^{2+}] + K_{FeOH^+}[Fe_{(aq)}^{2+}][OH^-] \\ & + K_{Fe(OH)_2^0}[Fe_{(aq)}^{2+}][OH^-]^2 + K_{Fe(OH)_3^-}[Fe_{(aq)}^{2+}][OH^-]^{3+} \\ & + K_{Fe(OH)_4^{2-}}[Fe_{(aq)}^{2+}][OH^-]^4 + K_{Fe^{II}L^0}[L^{2-}][Fe_{(aq)}^{2+}] \\ & + K_{Fe^{II}L_2^{2-}}[L^{2-}]^2[Fe_{(aq)}^{2+}] + K_{Fe^{II}L_3^{4-}}[L^{2-}]^3[Fe_{(aq)}^{2+}]. \end{aligned} \quad (50)$$

Mass balance equations for electron (e_T), quinone (S_T), iron (Fe_T), and oxalate (L_T) constitute four equations with four unknowns (E, $[Fe^{2+}]$, $[L^{2-}]$, and $[Z^0]$). At a given pH, equilibrium speciation of quinones and iron can be determined by solving for unknowns by iteration.

Fig. 10 shows the effects of added oxalate and malonate on the reduction of juglone by Fe^{II}. Hundred micromolar juglone is brought into contact with 500 μM Fe^{II} in the presence or absence of 5 mM oxalate or malonate. The total concentration of fully reduced juglone (X_T) is used as a measure of reaction progress when equilibrium is attained.

Earlier, we discussed the reaction of 100 μM juglone with 500 μM Fe^{II} (Fig. 9). As the pH was increased, concentrations of reduced juglone achieved at equilibrium (X_T) increased substantially. The addition of 5 mM malonate (Fig. 10) raises the pH required for $Fe^{III}(OH)_3$(s) precipitation and makes possible the production of modest amounts of reduced juglone between pH 3.2 and 5.5. These changes arise from the modest stabilization of Fe^{III} relative to Fe^{II} afforded by malonate. Oxalate is a stronger chelating agent than malonate, and therefore its effects are much more dramatic. Five millimolar of oxalate raises the pH required for $Fe^{III}(OH)_3$(s) precipitation even further, and achieves more than 80% conversion of oxidized juglone to reduced juglone between pH 3.0 and 5.0 (Fig. 10).

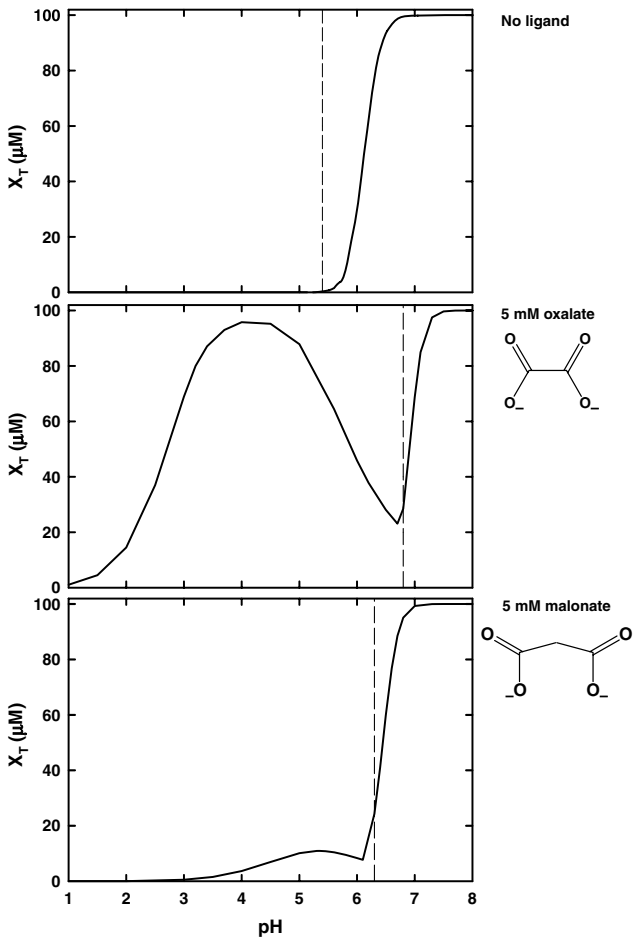

Fig. 10. Influence of added ligands on the reduction of juglone by Fe^{II}. Calculation conditions: 100 μM juglone (Z_T), 500 μM TOTFe^{II}, with or without 5 mM organic ligand. Vertical lines represent pH at which $Fe^{III}(OH)_3$(s,amorph) starts to form. The *y*-axis shows the reduced juglone concentration attained at equilibrium.

5. Conclusions

Reduction potentials for quinones and for iron are sufficiently close to one another that relatively minor changes in system constituents can have substantial effects on reaction progress. As far as quinones are concerned, electron-donating and electron-withdrawing substituents and side-groups engaging in protonation/deprotonation reactions alter standard reduction potentials and the slopes of reduction potential versus pH plots. As far as iron is concerned, increases in pH cause Fe^{III} and eventually Fe^{II} to precipitate. Plots of iron reduction potential as a function of pH, especially in the presence of aliphatic carboxylic acids, can become quite complex. It is noteworthy that oxalic acid and malonic acid dramatically extend the pH range where Fe^{II} oxidation by benzoquinones can take place. The influence of these and other biological exudates on redox reactions between quinone moieties within NOM and iron should not be overlooked. The agricultural and biogeochemical relevance of such reactions are likely considerable.

Acknowledgments

This project was supported by National Research Initiative Competitive Grant No. 2002-35107-11572 from the USDA Cooperative State Research, Education, and Extension Service.

Associate editor: George R. Helz

Appendix A. Supplementary data

Supplementary data associated with this article can be found, in the online version, at doi:10.1016/j.gca.2005.11.020.

References

Bailey, S.I., Ritchie, I.M., 1985. A cyclic voltammetric study of the aqueous electrochemistry of some quinones. *Electrochim. Acta* **30**, 3–12.

Bailey, S.I., Ritchie, I.M., Hewgill, F.R., 1983. The construction and use of potential-pH diagrams in organic oxidation–reduction reactions. *J. Chem. Soc. Perkin Trans. II*, 645–652.

Berson, J.A., 1988. *meta*-Quinonoid compounds. In: Patai, S., Rappoport, Z. (Eds.), *The Chemistry of the Quinonoid Compounds*, Vol. 2. Wiley-Interscience, New York, pp. 455–536.

Bruice, P.Y., 1998. *Organic Chemistry*. Prentice Hall, NJ.

Buerge, I.J., Hug, S.J., 1998. Influence of organic ligands on chromium(VI) reduction by iron(II). *Environ. Sci. Technol.* **32**, 2092–2099.

Capelle, S., Pellegrini, S., Cotelle, P., Imbenotte, M., Pommery, J., Catteau, J.P., 1996. Autoxidation of gentisic acid in aqueous media. *Water Res.* **30** (5), 1299–1303.

Clark, W.M., 1960. *Oxidation–Reduction Potentials of Organic Systems*. The Williams & Wilkins Company, Baltimore, MD.

Clemmer, J.D., Gilliland, B.L., Bartsch, R.A., Holwerda, R.A., 1979. Substituent effects on the electron-transfer reactivity of hydroquinones with Laccase Blue copper. *Biochim. Biophys. Acta* **568** (2), 307–320.

Cornell, R.M., Schwertmann, U., 1996. *The Iron Oxides: Structure, Properties, Reactions, Occurrence and Uses*. VCH Publishers, New York.

Deiana, S., Gessa, C., Marchetti, M., Usai, M., 1995. Phenolic acid redox properties: pH influence on iron(III) reduction by caffeic acid. *Soil Sci. Soc. Am. J.* **59**, 1301–1307.

Depew, M.C., Wan, J.F.K.S., 1988. Quinhydrones and semiquinones. In: *The Chemistry of the Quinoid Compounds*. Wiley-Interscience, New York, pp. 963–1018.

Dressler, H., 1994. *Resorcinol. Its Uses and Derivatives*. Plenum Press, New York.

Fukuzumi, S., Ishikawa, M., Tanaka, T., 1989. Acid-catalyzed reduction of *p*-benzoquinone derivatives by an NADH analogue, 9,10-dihydro-10-methylacridine. The energetic comparison of one-electron vs. two-electron pathways. *J. Chem. Soc. Perkin Trans. II*, 1811–1816.

Jones, D.L., 1998. Organic acids in the rhizosphere—a critical review. *Plant Soil* **205**, 25–44.

Kalusen, J., Trober, S.P., Haderlein, S.B., Schwarzenbach, R.P., 1995. Reduction of substituted nitrobenzenes by Fe(II) in aqueous mineral suspensions. *Environ. Sci. Technol.* **29**, 2396–2404.

Laidler, K.J., Meiser, J.H., 1999. *Physical Chemistry*. Houghton Mifflin Company, Boston, MA.

Lovley, D.R., 2001. Reduction of iron and humics in subsurface environments. In: Fredrickson, J.K., Fletcher, M. (Eds.), *Subsurface Microbiology and Biogeochemistry*. John Wiley, New York.

Lovley, D.R., Coates, J.D., Blunt-Harris, E.L., Phillips, E.J.P., Woodward, J.C., 1996. Humic substances as electron acceptors for microbial respiration. *Nature* **382**, 445–448.

Martell, A.E., Smith, R.M., Motekaitis, R.J., 2004. Critically Selected Stability Constants of Metal Complexes Database. U.S. Department of Commerce, National Institute of Standards and Technology.

Musso, H., 1967. Phenol coupling. In: Taylor, W.I., Battersby, A.R. (Eds.), *Oxidative Coupling of Phenols*. Marcel Dekker, New York, pp. 1–84.

Nurmi, J.T., Tratnyek, P.G., 2002. Electrochemical properties of natural organic matter (NOM), fractions of NOM, and model biogeochemical electron shuttles. *Environ. Sci. Technol.* **36**, 617–624.

Papelis, C., Hayes, K.F., Lechkie, J.O., 1988. HYDRAQL: A Program for the Computation of Chemical Equilibrium Composition of Aqueous Batch Systems.

Postma, D., Appelo, C.A.J., 2000. Reduction of Mn-oxides by ferrous iron in a flow system. *Geochim. Cosmochim. Acta* **64**, 1237–1247.

Rich, P.R., Bendall, D.S., 1980. The kinetics and thermodynamics of the reduction of cytochrome-*C* by substituted *P*-benzoquinols in solution. *Biochim. Biophys. Acta* **592** (3), 506–518.

Ritchie, J.D., Perdue, E.M., 2003. Proton-binding study of standard and reference fulvic acids, humic acids, and natural organic matter. *Geochim. Cosmochim. Acta* **67** (1), 85–96.

Roginsky, V.A., Pisarenko, L.M., Bors, W., Michel, C., 1999. The kinetics and thermodynamics of quinone–semiquinone–hydroquinone systems under physiological conditions. *J. Chem. Soc. Perkin Trans. II* (4), 871–876.

Schaap, W.B., Laitinen, H.A., Bailar, J.C., 1954. Polarography of Iron Oxalates, Malonates and Succinates. *J. Am. Chem. Soc.* **76** (22), 5868–5872.

Schwarzenbach, R.P., Stierli, R., Lanz, K., Zeyer, J., 1990. Quinone and iron porphyrin mediated reduction of nitroaromatic compounds in homogeneous aqueous-solution. *Environ. Sci. Technol.* **24** (10), 1566–1574.

Scott, D.T., McKnight, D.M., Blunt-Harris, E.L., Kolesar, S.E., Lovley, D.R., 1998. Quinone moieties act as electron acceptors in the reduction of humic substances by humics-reducing microorganisms. *Environ. Sci. Technol.* **32**, 2984–2989.

Sposito, G., 1989. *The Chemistry of Soils*. Oxford University Press, UK.

Steenken, S., Neta, P., 1982. One-electron redox potentials of phenols. Hydroxy- and aminophenols and related compounds of biological interest. *J. Phys. Chem.* **86**, 3661–3667.

Stone, A.T., 1997. Reactions of extracellular organic ligands with dissolved metal ions and mineral surfaces. In: Banfield, J., Nealson, K. (Eds.), *Geomicrobiology: Interactions Between Microbes and Minerals*. Mineralogical Society of America, Washington, DC, pp. 309–343.

Strathmann, T.J., Stone, A.T., 2001. Reduction of the carbamate pesticides oxamyl and methomyl by dissolved Fe^{II} and Cu^{I}. *Environ. Sci. Technol.* **35** (12), 2461–2469.

Strathmann, T.J., Stone, A.T., 2002. Reduction of oxamyl and related pesticides by Fe^{II}: influence of organic ligands and natural organic matter. *Environ. Sci. Technol.* **36** (23), 5172–5183.

Stumm, W., Morgan, J.J., 1996. *Aquatic Chemistry*. Wiley-Interscience, New York.

Thorn, K., Arterburn, J., Mikita, M., 1992. ^{15}N and ^{13}C NMR investigation of hydroxylamine-derivatized humic substances. *Environ. Sci. Technol.* **26**, 107–116.

Vyvyan, J.R., 2002. Allelochemicals as leads for new herbicides and agrochemicals. *Tetrahedron* **58**, 1631–1646.